CrossMark

TECHNICAL PAPER

Influence of the process parameters on the surface roughness, micro-hardness, and residual stresses in slide burnishing of high-strength aluminum alloys

J. T. Maximov[1] · A. P. Anchev[1] · G. V. Duncheva[1] · N. Ganev[2] · K. F. Selimov[1]

Abstract It is well known that apart from compressive residual stresses, smooth surface and microstructuring of the surface and subsurface layers are beneficial for enhancement of fatigue strength and load-carrying capacity of structural and machine components. This complex of properties can be achieved using surface severe plastic deformation. For symmetric rotational components made of high-strength aluminum alloys, slide burnishing is appropriate because of its simplicity and easy realization. The effect of the process parameters on the surface roughness, micro-hardness, and residual stresses obtained in slide burnishing of D16T aircraft aluminum alloy has been analyzed. The optimal values of the basic governing factors, which ensure minimum roughness (up to $0.05\,\mu$ m), have been established on the basis of a one-factor-at-the-time method, followed by a planned experiment and additional experiments. With the established combination of optimal values, the effect of number of passes and lubricant-cooler on the roughness, micro-hardness, and residual stresses in the surface being treated has been studied for two working schemes. To establish residual stress–depth profiles depending on the tool radius and burnishing force, FEM analysis of the slide burnishing process has been conducted. Thus, an evaluation of the effectiveness of slide burnishing as "mixed burnishing" has been made.

1 Introduction

It is common knowledge that the surface layers of structural and machine elements are most loaded during exploitation. The lifetime of the components depends on the quality of surface layers in the aspect of micro-structure, residual stresses and depth of distribution, micro-hardness, and roughness. The complex of these qualities is known as "surface integrity". Increasing the fatigue strength of the component requires a relevant technology for treating the surface layers, with which the required set of properties of these layers is achieved: grain refinement microstructure, residual compressive stress, maximum depth of the compressive zone, increased micro-hardness, minimal roughness. Finishing by cutting introduces residual tensile stresses. That is why the desired set of properties of the surface layer can be achieved by surface plastic deformation (SPD). The latter is mechanical treatment of the surface layer by means of a hard indenter which is compressed normally to the machined surface of the metal workpiece with a ductile behavior, causing plastic deformation of the surface layer at the spot contact. The methods implementing SPD can be classified under different features. According to the effect that needs to achieved, the world leader Ecorol defines two processes: roller burnishing and deep rolling. The main objective of the first is to produce "burnishing", wherein the roughness is reduced considerably—for example, some tools achieve mirror surfaces. The other attributes of the surface layer (increased micro-hardness and compressive residual stresses) inherent in the SPD also

Technical Editor: Márcio Bacci da Silva.

✉ J. T. Maximov
jordanmaximov@gmail.com

[1] Technical University of Gabrovo, 5300 Gabrovo, Bulgaria

[2] Czech Technical University in Prague, Prague, Czech Republic

3068

J Braz. Soc. Mech. Sci. Eng. (2017) 39:3067–3078

exist but are rather concomitant and not significant. Deep rolling aims to produce three effects simultaneously: burnishing, cold work, and compressive residual stresses with maximum intensity and of considerable depth. The majority of studies are aimed at investigating the effects of roller burnishing [1–14]. The increased fatigue life performance of relevant components achieved through deep rolling has been less studied [15–19].

High-strength aluminum alloys (7075-T6, 2024-T3, 2324-T39, D16T, D16AT, 1163T7) possess sufficient strength at a relatively low weight, a large corrosion resistance, and good workability. Because of that, they are widely used in responsible structures in various industries, including the aircraft building, due to their optimal combination of physical and mechanical properties [20]. To improve the surface integrity of structural components made of aluminum alloys, SPD has been applied successfully [1–3, 5, 6, 21–34]. Basically, the studies aimed at evaluating the effectiveness of roller burnishing on the obtained roughness and accuracy [1–3, 5, 6, 28, 29], as well as of deep rolling [27, 30, 31] for increasing the fatigue strength.

A relatively small part [23–26] of the studies is dedicated of slide diamond burnishing of aluminum alloys and only [26] relates to high-strength alloys—aluminum matrix composites. In this method, the tangential contact between the deforming element and the workpiece surface is a sliding friction.

A modern trend is to improve the mechanical properties of the surface layers of aluminum alloys by modifying their micro-structure. The modification consists in refining grains, reducing the pores in the material and homogenization of the structure. It is implemented using tangential a sliding contact between a deforming element and the surface being treated, to provoke a severe plastic deformation of the surface layer. Thus, the micro-structured layer has greatly increased plasticity, high-yield limit, and tensile strength. This concept is known [35–40] as "Friction Stir Processing" (FSP).

It is obvious that SPD using tangential sliding contact with a suitable combination of process parameters can lead not only to small roughness but, at least partially, to the beneficial effects of FSP. For symmetric rotational components made of high-strength aluminum alloys, slide burnishing is appropriate because of its simplicity and easy realization. It combines the advantages of smooth burnishing, deep rolling, and friction stir processing.

The main objective of this study is to establish the effect of the process parameters on the surface roughness, micro-hardness, and residual stresses obtained in slide burnishing of D16T aircraft aluminum alloy and thus, an evaluation of the effectiveness of slide burnishing as "mixed burnishing" to be made.

2 Experiment

2.1 Formulation of the experiment

2.1.1 Governing factors

The governing factors of the slide burnishing process are the following: basic—sphere radius of the diamond r, mm; burnishing force F_b, N; feed rate f, mm/rev; burnishing velocity v, m/min and additional—number of passes N; lubricant-cooler.

2.1.2 Essence of the experiment

An extended experiment to determine the roughness obtained by slide burning was carried out. The experiment consists of three stages. In the first stage, a one-factor-at-the-time methodology was applied to screen the significant basic factors and their levels. In the second stage a planned experiment with a large number of experimental points and number of factor levels more than three were conducted. By means of a regression analysis, a mathematical model of the obtained roughness was established. The model (the hyper-surface) was studied through a method of the sections with hyper-planes and the area of basic governing factors which ensures minimum values of the roughness was found. In the third stage, through additional experiments, the combination of optimal values of the governing factors, which ensures the smallest roughness, was selected. Further, with the selected combination of basic governing factors, the effects of the additional factors on the obtained surface roughness, micro-hardness, and residual stresses were investigated.

2.2 Experiment details

2.2.1 Machine tool and slide burnishing device

The experiment was conducted on CNC T200 lathe (Fig. 1). A special burnishing device was designed and manufactured (Fig. 2). The device is mounted on the tool post of the lathe. A polycrystalline diamond tool with spherical tip is supported elastically in the device. The required burnishing force was set by deforming an axial spring with linear behavior, situated in the device. The diamond burnishing point is brought into contact with the specimen at its centerline and normal to the surface being treated. The device is then fed into the specimen an additional 0.05 mm to allow the diamond tool to become disengaged from the stop in the device. The latter is then fed along the surface of the rotating specimen to produce a burnished surface.
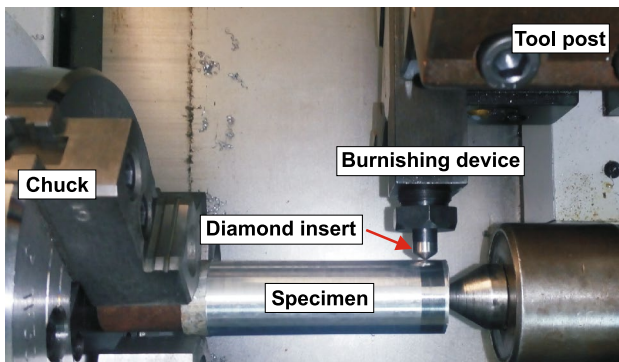
A lubricant–cooler Hacut 795-H was used.

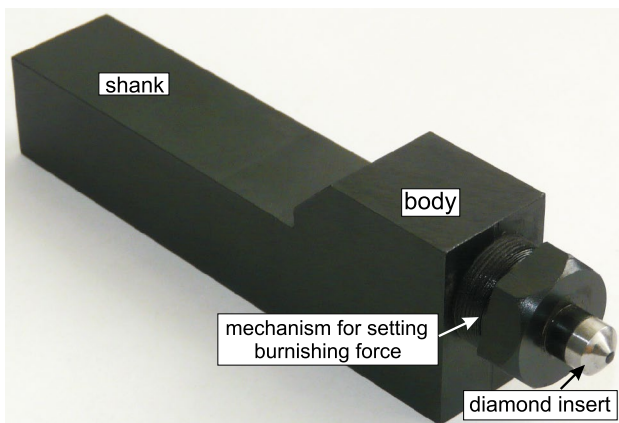**Fig. 1** Slide burnishing implementation on CNC lathe

Fig. 2 Slide burnishing device

2.2.2 Specimens

Machining trials were carried out on the specimens made of D16T aluminum alloy, which has a wide range of applications in the industry. Tensile tests on specimens with diameter $d = 6$ mm and base $\ell = 6\,d$ recorded the following average mechanical characteristics: Young's modulus $E = 0.7 \times 10^5$ MPa; yield limit $\sigma_Y = 348$ MPa; ultimate stress $\sigma_u = 501$ MPa; elongation $A_5 = 10.4$ %; transversely contraction $z = 33$ %. The measured hardness was 110 HB.

The specimens have a length of 200 mm and diameter of 32 mm. Each specimen was clamped to one side with the chuck and supported on the other side according to Fig. 1. Turning as premachining and slide burnishing were carried out in one clamping process to minimize the concentric run-out in burnishing. The turning was conducted from end to end of each specimen, while the treated length through slide burnishing with one combination of governing factors was 20 mm. Thus, for a group of experimental points

(combinations of governing factors) one and the same initial roughness before burnishing was ensured.

DNMG 50608–RF carbide cutting insert was used for turning. Premachining was conducted with a constant feed rate $f = 0.1$ mm/rev, cutting speed $v_c = 90\ m/$min, and cutting depth $a_p = 0.25$ mm. The cutting edge radius was $r_c = 0.8$ mm.

The surface roughness on R_a criterion in axial direction was measured using Mitutoyo Surftest—4. Each experimental value of R_a was obtained in the following way: the measurement was taken on three generatrixes at 120^0 as for each generatrix the mean value of the roughness was given; the final value of the roughness was obtained as an arithmetic mean of the obtained roughness for the three generatrixes.

The average roughness after turning on R_a criterion was 0.445 µm.

After slide burnishing, micro-hardness–depth profiles were measured on cross-section specimens applying HV 0.05 hardness testing. RMT-3 micro-hardness tester was used.

The largest contribution to the increase of fatigue life of axes and shafts subjected to cyclic bending have the residual axial normal stresses introduced in the surface layer via slide burnishing. These stresses were measured by means of x-ray diffraction method. Diffraction measurements were carried out on a vertical θ/θ X'Pert PRO MPD diffractometer with a pin-hole collimator 0.5×1.0 mm^2 in the primary beam. Positioning of the measured sample to the required locations was done by combining versatile positioning system with six degrees of freedom and laser triangulation for precise surface position determination with accuracy of approximately 5 µm. Since the effective penetration depth of used Cr$K\alpha$ radiation into the investigated steel is only approximately 8 µm, a biaxial state of stress was assumed, and the "sin$^2\psi$" method with least squares fitting procedure was used to evaluate residual stresses. The measured diffraction profile of Al {311} planes has for the used filtered Cr$K\alpha$ radiation its maximum at 2θ ≈ 139.5°. Diffraction profiles were fitted by Pearson VII function, and lattice deformations were calculated. In the generalized Hooke's law, X-ray elastic constants $-s_1 = 4.89 \times 10^{-6}$ MPa^{-1} and ½$s_2 = 19.05 \times 10^{-6}$ MPa^{-1} were utilized. Moreover, the diffraction profile corresponding to Al {311} planes parallel with the surface was characterized by FWHM (Full Width at Half Maximum) profile parameter which could be interpreted as "degree of plastic deformation", because the diffraction profile broadening relates to such material characteristics as grain size, microscopic residual stresses or dislocation density whose evolution is closely connected with plastic deformation.

3070

J Braz. Soc. Mech. Sci. Eng. (2017) 39:3067–3078

Table 1 Machining parameters for slide burnishing

Process parameter	Levels				
Sphere radius of the diamond r, mm	1	2	3	4	5
Burnishing force F_b, N	50	100	150	200	250
Feed rate f, mm/rev	0.05	0.075	0.1	0.125	0.15
Burnishing velocity v, m/min	50	75	100	125	150

3 Results and discussions

3.1 Roughness obtained

3.1.1 First stage

The machining parameters for slide burnishing and diamond sphere radii are depicted in Table 1.

The influence of each of the basic governing factors on the obtained roughness is evaluated, and the remaining three factors have constant values. The outcomes for the obtained roughness are depicted in Fig. 3. For all combinations of governing factors in which the radius r is equal to 1 mm, strongly deteriorated roughness was obtained—much higher than the initial roughness. These outcomes (for $r = 1$ mm) are not displayed in Fig. 3 and in the next study stage this level of the factor r is excluded from the experiment. When the radius increases to 4 mm, the obtained roughness decreases, then begins to rise. Apparently, the radius r has the strongest influence, while the burnishing velocity v has the least influence on the roughness. It is also obvious that the correlation between the radius r and burnishing force F_b is most pronounced. This fact has a clear physical sense: the increased force and reduced radius lead to bigger depth of penetration and vice versa. It is noteworthy that the feed rate f in its own right has a little impact on the obtained roughness. However, its correlation with the radius r is more pronounced—the maximum radius for small and large feed rate values deteriorates the roughness.

3.1.2 Second stage

Based on the results from the first stage, in this study stage, a planned experiment has been carried out. By means of QstatLab [41], an experimental design has been synthesized. It consists of 76 experimental points as 16 of them are in the vertices of the hypercube factor space. The governing factors and their levels are shown in Table 2.

The factors measured in natural physical units are marked with $\tilde{x}_i$. During the experiment each of the factors $\tilde{x}_i$ alters in a given interval $\tilde{x}_{i,min} \leq \tilde{x}_i \leq \tilde{x}_{i,max}$. The lower limit $\tilde{x}_{i,min}$ of this interval is called lower level, the upper one $\tilde{x}_{i,max}$ is upper level and the middle $\tilde{x}_{i,0}$ of this interval is the factor's basic level. The factors used in the experiment have different dimensions. To eliminate the experimental plan's dependence from the dimensions, the factors $\tilde{x}_i$ are transformed into a coded form x_i through dependence.

$$x_i = \left(\tilde{x}_i - \tilde{x}_{i,0} \right) / \left| \tilde{x}_{i,max} - \tilde{x}_{i,0} \right| \tag{1}$$

Through QstatLab a regression analysis of the obtained experimental results is carried out. For the objective function (roughness R_a obtained after slide burnishing) a polynomial of fourth order.

$$\begin{aligned}
R_a = {} & 0.12893 + 0.18112x_1^2 - 0.06085x_1^3 + 0.07208x_2^4 \\
& + 0.04537x_1^2x_3 - 0.04081x_2x_3x_4^2 \\
& + 0.06381x_1^2x_2 + 0.17363x_1^3x_2 - 0.16635x_1x_2^3 \\
& - 0.10057x_1x_3x_4^2 - 0.08353x_2^2x_3^2
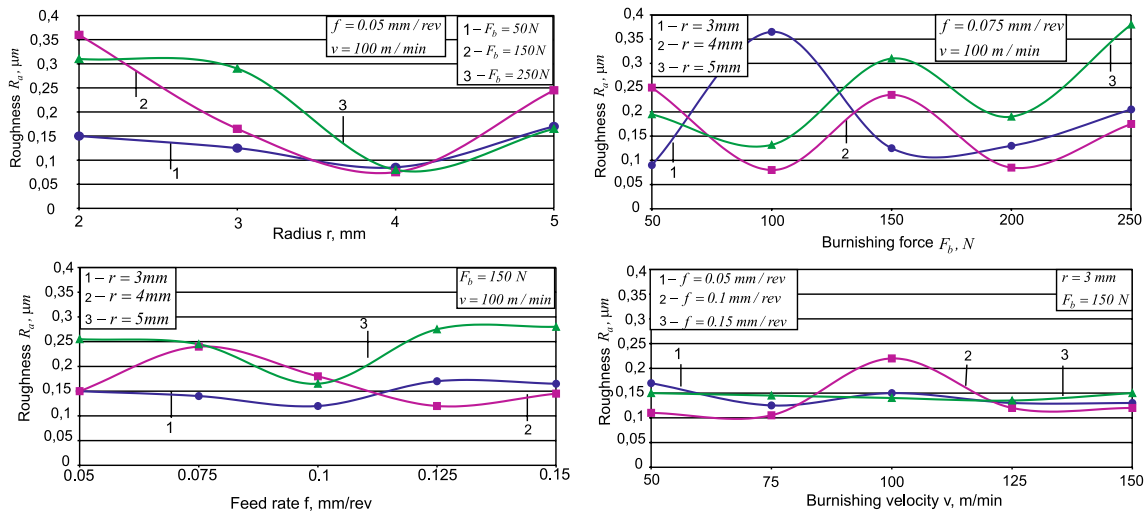\end{aligned} \tag{2}$$

Fig. 3 Outcomes from one-factor-at-the time experiment

Table 2 Governing factors and their levels

Governing factors Naturals $\tilde{x}_i$	Coded x_i	Levels of the factors				
		Coded for the first factor				
		−1	−0.333	+0.333		+1
		Coded for the remaining factors				
		−1	−0.5	0	+0.5	+1
		Natural				
Sphere radius of the diamond r [mm], $\tilde{x}_1$	x_1	2	3	4		5
Burnishing force F_b [N], $\tilde{x}_2$	x_2	50	100	150	200	205
Feed rate f [mm/rev], $\tilde{x}_3$	x_3	0.05	0.075	0.1	0.125	0.15
Burnishing velocity v [m/min], $\tilde{x}_4$	x_4	50	75	100	125	150

is obtained, where x_i is determined by dependence (1).

Equation (2) has an empirical nature since it is obtained by an experimental way and a regression analysis on the basis of an experimental design.

To estimate the significance of the governing factors as well as the interaction between them, the factors are presented in coded mode (dimensionless) in the regression model in accordance with Eq. (1). Each factor is changed in the interval $-1 \leq x_i \leq 1$. Then the coefficients in Eq. (2) have the dimension of the objective function, and the absolute values of these coefficients are a measure of the importance of the factors as well as the interaction between them. For instance, the interaction between the factors x_1 and x_2 is most greatly expressed, which has a clear physical meaning. Using a deforming element with a small radius and larger burnishing force leads to very high surface pressure resulting in a deeper penetration in the surface layer. Moreover, an adhesion of specimen material on the deforming element has been observed.

Figure 4 shows sections of the hyper-surface of the roughness-obtained model with different hyper-planes. The conclusion, that the diamond radius r has the biggest influence on the roughness and the burnishing velocity v–the smallest influence, has been corroborated.

The search review of Fig. 4 shows that the minimum roughness is ensured by the following combination of basic governing factors: $r = 3 \div 4$ mm, $F_b = 150 \div 200N$, $f = 0.05$ mm/rev, $v = 100$ m/min. In the third stage the optimal values of r and F_b are found by means of additional experiments.

3.1.3 Third stage

Figure 5 shows the results from additional experiments for determination of the optimum values of radius r and burnishing force F_b. Obviously, the minimum roughness is obtained for $r = 4$ mm, $F_b = 200N$, $f = 0.05$ mm/rev, $v = 100$ m/min. With the established optimal values of

the basic governing factors, the influence of the number of passes on the obtained roughness has been studied for two working schemes (Fig. 6): one-way and two-way. As Fig. 7a shows, the first scheme ensures smaller roughness. By increasing the number of passes, a monotonically decreasing roughness is observed. In the case of a two-way scheme, the tendency is disparate: after two passes the roughness slightly decreases, after which sharply increases.

Figure 7b depicted the outcomes for the obtained roughness without using a lubricant-cooler (dry slide burnishing). As might be expected, the roughness is larger in comparison with that in Fig. 7b. However, after second and after eighth passes, the roughness decreases in the case of a one-way working scheme. As a whole, the two-way working scheme ensures considerably lower roughness.

The outcomes for the roughness in Fig. 7 raise questions about the influence of the number of passes on the micro-hardness and residual stresses in the surface layers.

3.2 Micro-hardness

3.2.1 Experimental outcomes

The effects of various working schemes and number of passes of slide burnishing on the micro-hardness–depth profiles are illustrated in Fig. 8. For both working schemes, irrelevant whether lubricant-cooler has been used, maximum micro-hardness values were measured below the surface layer—at a depth of approximately 100 μm. The maximum magnitude of the micro-hardness to a depth of about 100 μm may be explained by the mechanism of the surface plastic deformation. In the surface layer the metal flows from the peaks to the valleys, filling the valleys. The plastic deformation is terminated when the metal, located immediately below the valleys, reaches the maximum possible strain hardening. For the combination „one-way scheme–lubricant", the maximum micro-hardness was obtained after the first past (Fig. 8a). The increase was from
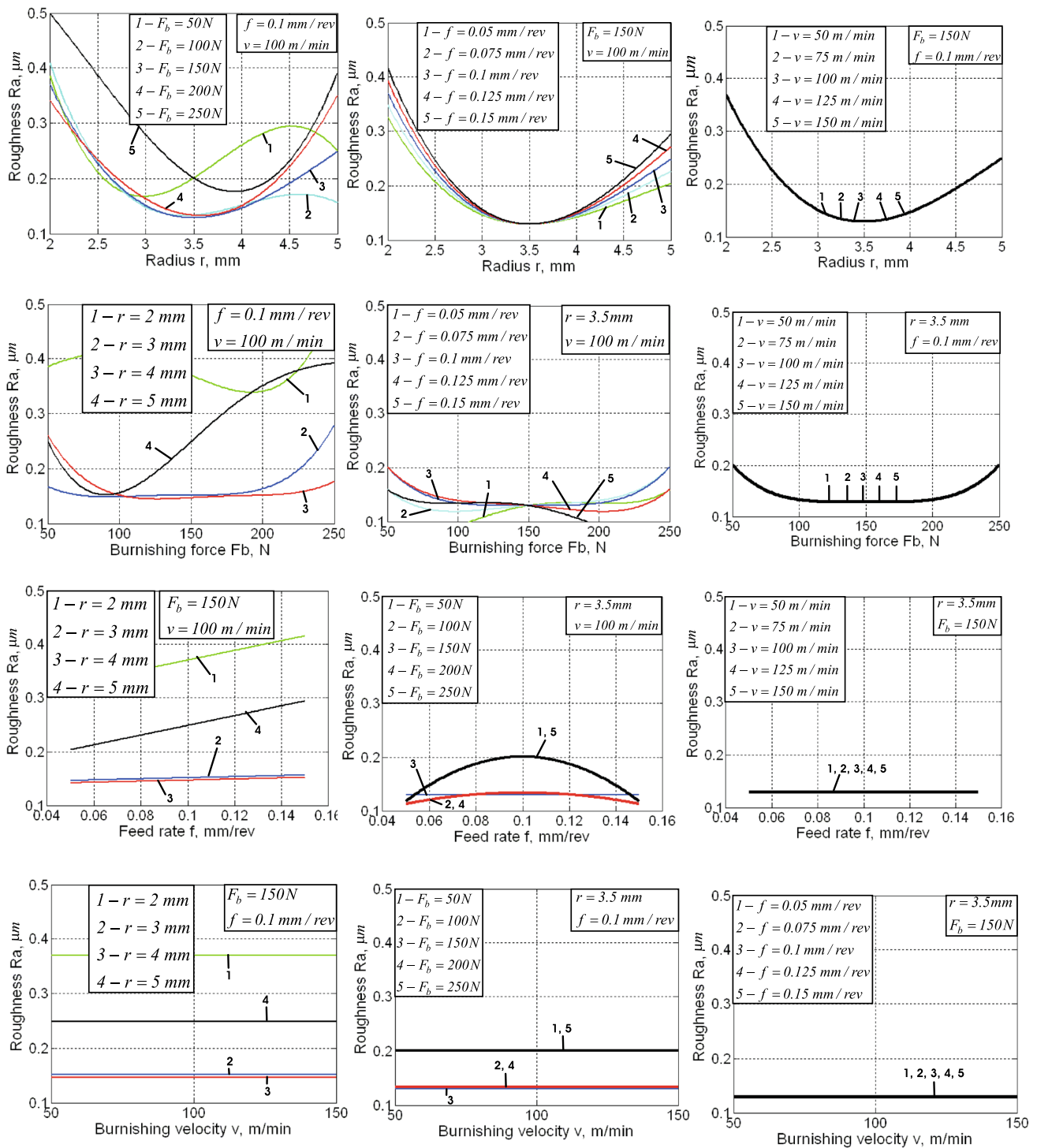
Fig. 4 Sections of the hyper-surface of the roughness obtained model with different hyper-planes

125 to 170 units according to Vickers. With increasing the number of passes insignificant softening was observed. The opposite trend was observed in two-way scheme (Fig. 8b). With an increase in the number of passes the micro-hardness increases, as the measured maximum value is 188 HV,

i.e., the increase against the base (125HV) is 50.4 %. Dry slide burnishing (Fig. 8c) shows similar trends to those seen in slide burnishing with lubricant. In the variant "one-way scheme" the softening effect is considerably more pronounced. In the variant "two-way scheme" (not shown in
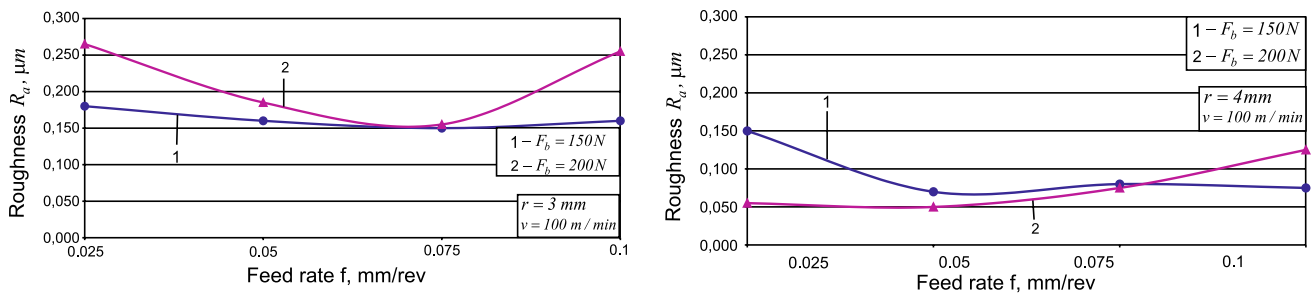
Fig. 5 Influence of the radius and burnishing force on the roughness obtained

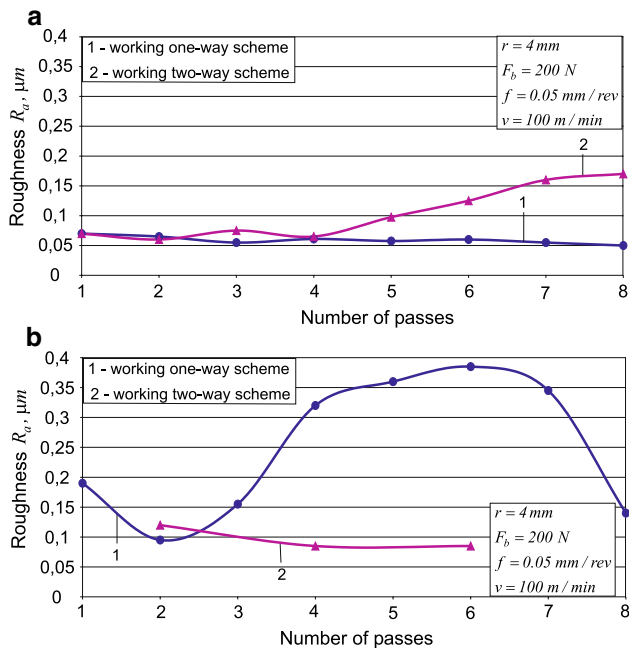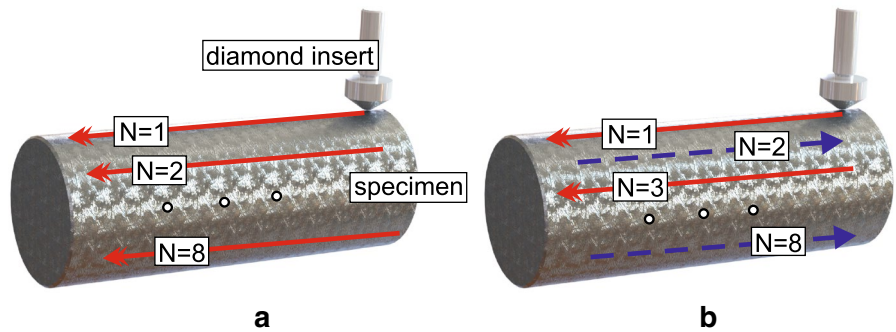**Fig. 6** Slide burnishing working schemes: **a** one-way; **b** two-way

Fig. 7 Effect of number of passes and working scheme on the roughness obtained: **a** with lubricant; **b** dry slide burnishing

Fig. 8) a slight increase in micro-hardness was observed with increasing the number of passes.

It is quite possible for the "manufacturing heredity factor" (production of the initial bar stocks, precipitation of the alloy, and so on) to influence on the micro-hardness distribution. However, the purpose of the study was to evaluate the effect of slide burnishing on the obtained micro-hardness by comparing it with a sample that was processed only by cutting (reference condition). The "manufacturing heredity factor" influences in the same way the compared specimens (reference condition and burnished specimens).

3.2.2 FEM simulations of the equivalent plastic strain (cold work) in surface and subsurface layers

The increased micro-hardness, experimentally determined in Sect. 3.2.1, is a result of the plastic deformation of the surface and subsurface layers. There is therefore a correlation between the micro-hardness–depth profile and equivalent plastic strain–depth profile.

To establish the equivalent plastic strain–depth profiles depending on the tool radius and burnishing force, FEM analysis of the slide burnishing process was conducted. ABAQUS/CAE 6.12 was used. 3D FE model was developed (Fig. 9). The modeled part (because of the symmetry only a half part has been modeled) from the workpiece consists of 2260 eight-nodal hexahedral FEs of type C3D8R and 200 linear wedge FEs of type C3D6. Total number of nodes is 2856. A rigid ball exerts compression on the workpiece surface until the compression force reaches a prescribed magnitude. After that the ball is raised and moved along the workpiece axis to a distance $f = 0.05$ mm that

3074

J Braz. Soc. Mech. Sci. Eng. (2017) 39:3067–3078

Fig. 8 Micro-hardness—depth profile at various conditions: **a** lubricant—one-way scheme; **b** lubricant—two-way scheme; **c** without lubricant–one-way scheme
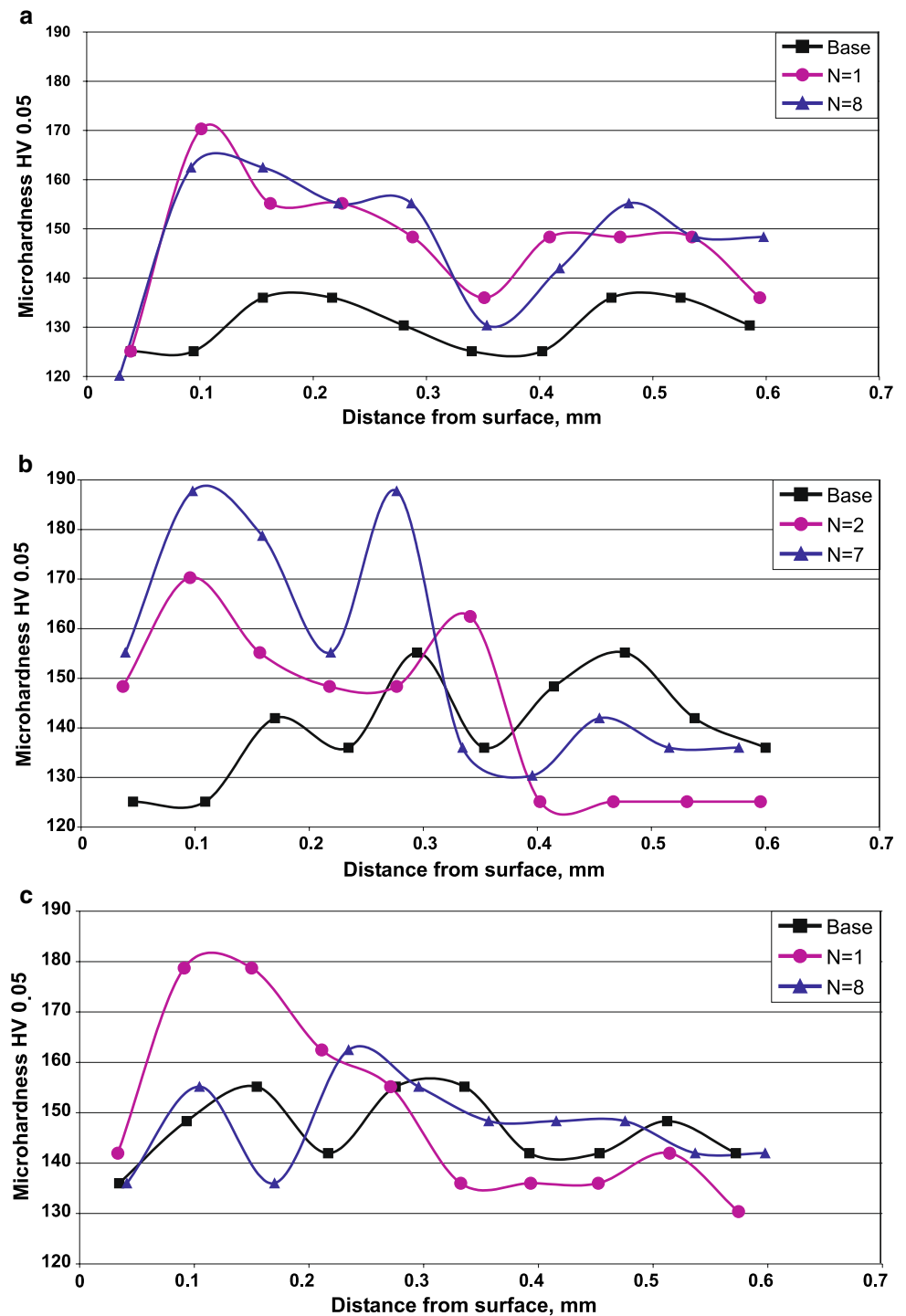
is equal to the feed rate. This cycle "loading–unloading–moving" is repeated twenty times. A displacement control was used as a time curves for the tool normal and axial displacements.

To obtain a reliable FE model, apart from a realistic geometry and interactions, an adequate constitutive model of the behavior of the workpiece surface layers is also needed. The constitutive model defines the dependence between stress and strain tensors. In the burnishing theory, the "flow stress" concept is used to give this dependence for the surface layer in the plastic field. The burnishing process acts on the surface layer of the workpiece. The behavior of this layer considerably differs from the bulk material, because of the existence of large plastic strains, as well as specific micro-profiles and other effects created in the production of the workpiece. For these reasons the
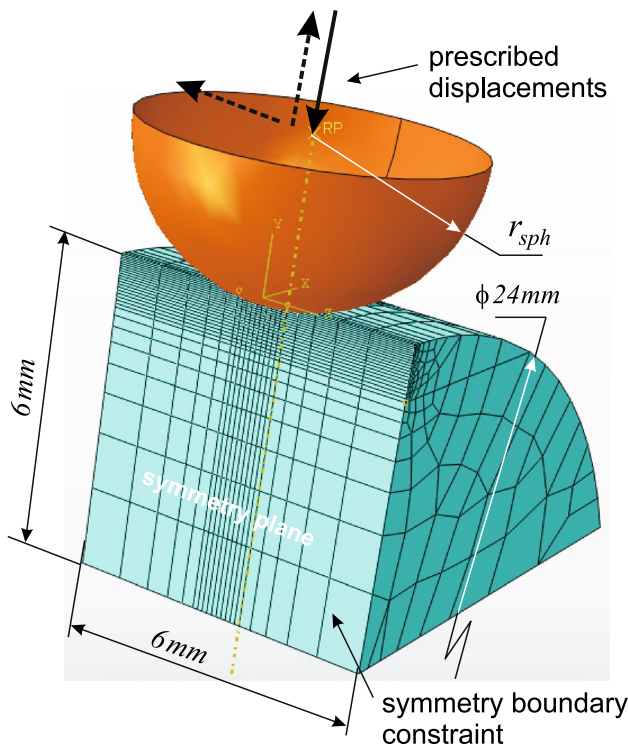
Fig. 9 3D FE model of slide burnishing

conventional testing methods for stress–strain curve determination by a one-dimensional test, as well as the corresponding cyclic tests, can be applied to the bulk material, but not to the surface layer. For the surface layer this dependence in the plastic field must be determined in a manner that corresponds to the actual loading of this layer. A combined approach, based on experimental test (instrumented indentation test) and inverse FEM analysis, was used. The experimental part of the approach is a test, similar to the method for measuring Brinell hardness. An indenter, having diameter of the sphere $d_{sph} = 2.5$ mm, is pressed in the specimen under the action of axial force P_a

(Fig. 10). After unloading, the residual depth of penetration d_p^{res} of the spherical tip is established. The dependence $P_{a,i} = P_{a,i}\left(d_{p,i}^{res}\right)$ is obtained in tabulated form. FE analysis of the indentation test aims to establish the relationship stress–strain of the workpiece material in the plastic field. This dependence is presented in the form:

$$\sigma = \sigma_Y \left(1 + \frac{E}{\sigma_Y}\varepsilon_P\right)^n, \tag{3}$$

where σ is the flow stress, σ_Y is the yield limit, E is Young's modulus, ε_P is the plastic strain, and n is the strain hardening for a one-dimensional stressed state.

FE simulation (axisymmetric FE model) of the mechanical test is carried out repeatedly, each time with different combinations of σ_Y and n in the model (3), and from the FE results for each combination the dependence "axial force-residual depth of the sphere imprint" is established. The imprint diameter was measured and the residual depth was calculated. This dependence is compared with the experimental one. Variation with the pair σ_Y and n continues until the difference between the experimental and the FE dependencies is minimized (Table 3). However, Eq. (3) describes hardening in the plastic field in conditions of a 1D stressed state and it is assumed that this equation is valid for all possible loading paths and stressed states. In fact, the deforming process is a 3D process. This cyclic loading (one cycle "loading–unloading") causes deformation anisotropy; that is irregular movement of the yield surface in the stress space. That is why, nonlinear kinematic hardening law was chosen in the axisymmetric FE model. For the constants in Eq. (3), the following was obtained: $E = 72$ GPa; $\sigma_Y = 280$ MPa; $n = 0.075$.

Because of the cyclic loading in vicinity of a point from the surface being burnished, nonlinear kinematic/isotropic hardening was assigned in the 3D FE model (Fig. 9). The kinematic hardening component used alone predicts plastic shakedown after one cycle, while the isotropic component in combination with the nonlinear kinematic component
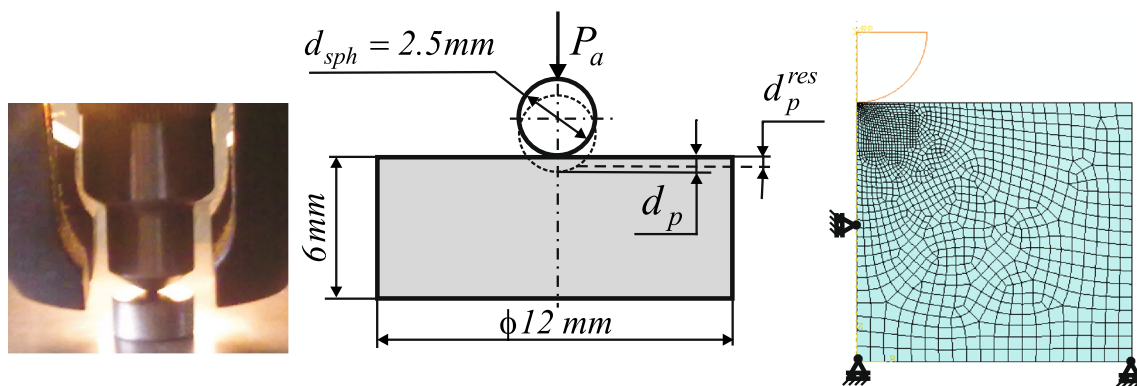

Fig. 10 Photo, scheme, and FE model of the indentation test

Table 3 Axial force-residual depth of the sphere imprint dependences

Axial force P_a, N	Experiment	49.05	98.10	147.15	196.2	294.3
	FEM	49.19	98.21	147.22	196.6	294.22
Depth d_p^{res}, mm	Experiment	0.0065	0.0128	0.0195	0.0289	0.0362
	FEM	0.0061	0.0124	0.0188	0.0225	0.0351

Table 4 Depth of penetration depending on the tool radius and burnishing force

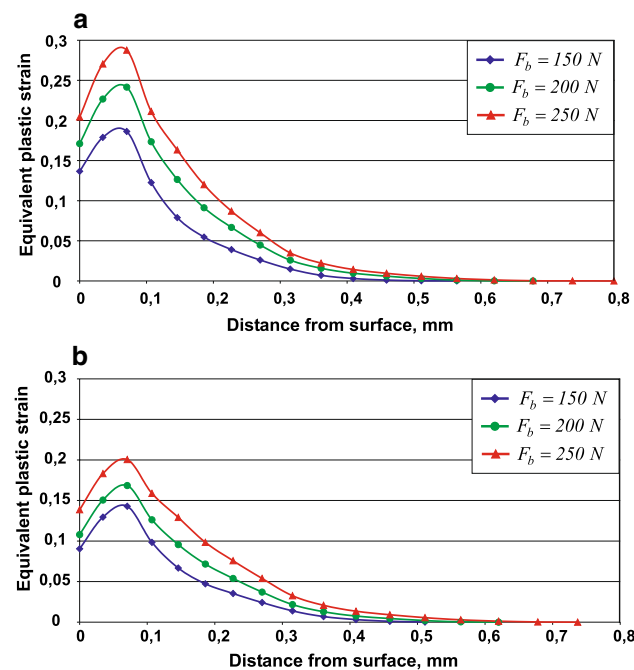| Burnishing force F_b, N	150	200	250
Depth of penetration d_p, mm			
$r = 3$ mm	0.01367	0.01816	0.02148
$r = 4$ mm	0.01216	0.01516	0.01876

Fig. 12 Residual surface axial stress

Fig. 11 Equivalent strain distribution in a depth: **a** $r = 3$ mm; **b** $r = 4$ mm

predicts the material plastic behavior after several cycles. The Poisson's ratio is 0.33. The depth of penetration depending on the tool radius and burnishing force was established through 3D FE model (Table 4).

The FE outcomes for the equivalent strain distribution in a depth are shown in Fig. 11. The dependence between strain hardening and hardness, respectively micro-hardness, is well known. The FE outcomes for the equivalent plastic strain show that its maximum value is not at the points of the surface, but several ten micrometers below the surface. Therefore, the maximum micro-hardness is of the same distance from the surface layer. For all combinations
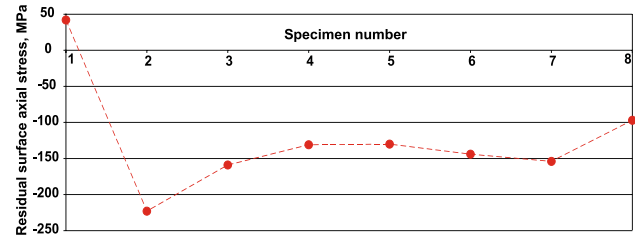
of radii and burnishing forces, the maximum values of the equivalent plastic strain have been obtained under the surface layer at a depth between 50 and 100 micrometers. This fact confirms the correlation between the micro-hardness and the equivalent plastic deformation.

For both magnitudes of the tool radius, the equivalent plastic strain in surface and subsurface layers increases as the burnishing force is growing. The smaller radius ensures greater plastic deformation. If the objective of the slide burnishing is to achieve greater micro-hardness, therefore a smaller radius and larger burnishing force should be selected.

The used 3D FE model does not include the initial workpiece roughness, and the initial stressed and strained state includes zero values of stresses and strains. Nevertheless, this model adequately presents the deformation process due to the adequate constitutive model of the material.

3.3 Residual axial stresses

3.3.1 X-ray stress analysis

Figure 12 shows the effect of working schemes and lubricant–cooler on the surface residual axial normal stresses. Specimen 1, called "basic", was processed only by cutting. The remaining samples, after cutting, were subjected to slide burnishing, as it was described in Sect. 2.2.2, as follows: specimen 2 (S2)–with lubricant and number of passes $N = 1$; S3–with lubricant, one-way scheme and $N = 8$; S4–with lubricant, two-way scheme and $N = 2$; S5–with lubricant, two-way scheme and $N = 6$; S6–without lubricant and $N = 1$; S7–with lubricant, one-way scheme and $N = 8$; S8–with lubricant, two-way scheme and $N = 4$. Slide burnishing was carried out using optimal basic

parameters: $r = 4$ mm; $F_b = 200$ N; $f = 0.05$ mm/rev; $v = 100$ m/min.

Apparently, the residual surface axial stresses in the basic specimen are tensile, while the slide burnishing introduces compressive residual axial stresses in the surface layer. The largest absolute values of residual surface axial stresses were obtained for specimen S2. With increasing the number of passes up to $N = 8$ (specimen S3), the residual stresses decrease in absolute value because of the deforming anisotropic due to the cyclic loading in vicinity of a point from the surface being burnished. This is the reason for the residual stress relaxation. The comparison between S2, S4, and S5 shows that the relaxation is biggest after the first cycles (see S2 and S4), after which the relaxation rate slows sharply (see S4 and S5). For the case of dry slide burnishing (see S6, S7, and S8), the two-way scheme (S8) apparently leads to a more intensive residual stress relaxation.

3.3.2 FEM residual stress analysis

To establish the residual axial stress–depth profiles depending on the tool radius and burnishing force, FEM analysis of the slide burnishing process was conducted using the FE model shown in Fig. 9. The role of the initial roughness (after turning) in the FE model is very important for the resulting characteristics (after burnishing) in the surface layer. However, the used 3D FE model aims to provide information about the depth of the zone with beneficial residual compressive stresses, since in the surface layer these stresses were measured experimentally.

The FE outcomes for the residual axial stress distribution are shown in Fig. 13. For both magnitudes of the tool radius, the depth of the beneficial residual compressive zone increases when the burnishing force grows. Although it is insignificant, this tendency is more pronounced for the smaller radius. For both radii the increase of burnishing force leads to reduction of the surface residual stresses in absolute value, excluding the combination $r = 4$ mm and $F_b = 150$ N. Simultaneously, the intensity of the compressive zone grows. For the optimal magnitudes of the governing factors, respectively, $r = 4$ mm and $F_b = 200N$, the compressive zone depth is 0.52 mm, which is a significant depth for smooth burnishing.

4 Conclusions

The results from the expanded experimental study show that slide burnishing of high-strength aluminum alloys significantly reduces surface roughness—up to 0.05 µ m. Therefore, this method fulfills the requirements for "smooth burnishing". Furthermore, slide burnishing of
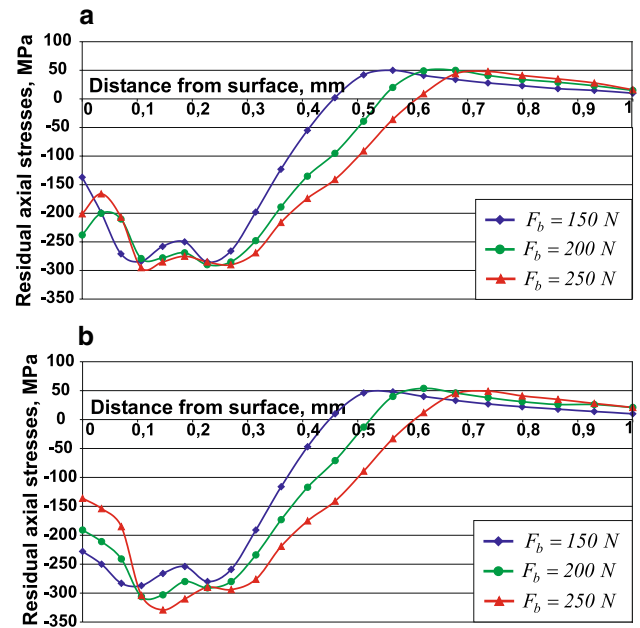

Fig. 13 Residual axial stress distribution: **a** $r = 3$ mm; **b** $r = 4$ mm

these alloys introduces compressive residual stresses in the surface and subsurface layers which are close to the yield limit in a depth more than 0.5 mm. The micro-hardness immediately under the surface layer was also significantly increased. Therefore, slide burnishing of high-strength aluminum alloys can be implemented as "mixed burnishing" according to the classification made by Korzynski [42].

References

1. El-Axir MH et al (2008) Improvements in out-of-roundness and microhardness of inner surfaces by internal ball burnishing process. J Mater Process Tech 196(1–3):120–128
2. John MRS, Vinayagam BK (2014) Optimization of nonlinear characteristics of ball burnishing process using Sugeno fuzzy neural system. J Braz Soc Mech Sci Eng 36:101–109
3. Basak H, Goktas HH (2009) Burnishing process on al-alloy and optimization of surface roughness and surface hardness by fuzzy logic. Mater Des 30(4):1275–1281
4. El-Taweel TA, El-Axir MH (2009) Analysis and optimization of the ball burnishing process through the Taguchi technique. Int J Adv Manuf Technol 41:301–310
5. El-Tayeb NSM et al (2009) On the surface and tribological characteristics of burnished cylindrical Al-6061. Tribol Int 42(2):320–326
6. El-Tayeb NSM et al (2007) Influence of roller burnishing contact width and burnishing orientation on surface quality and

tribological behaviour of Aluminium 6061. J Mater Process Tech 186(1–3):272–278

7. Hua W et al (2008) Contact force studies of a burnishing slider. Tribol Int 41(1):60–66

8. El-Axir MH (2000) An investigation into roller burnishing. Int J Mach Tool Manu 40(11):1603–1617

9. Malleswara RJN et al (2010) The effect of roller burnishing on surface hardness and surface roughness on mild steel specimens. Int J Appl Eng Res 1(4):777–785

10. Shiou FJ, Cheng CH (2008) Ultra-precision surface finish of NAK80 mould tool steel using sequential ball burnishing and ball polishing processes. J Mater Process Tech 201(1–3):554–559

11. Shiou FJ, Hsu CC (2008) Surface finishing of hardened and tempered stainless tool steel using sequential ball grinding, ball burnishing and ball polishing processes on a machining centre. J Mater Process Tech 205(1–3):249–258

12. Shiou FJ, Ciou HS (2008) Ultra-precision surface finish of the hardened stainless mold steel using vibration-assisted ball polishing process. Int J Mach Tool Manu 48(7):721–732

13. Thamizhmanii S et al (2008) Surface roughness investigation and hardness by burnishing on titanium alloy. J Achiev Mater Manu Eng 28(2):139–142

14. Yeldose BC, Ramamoorthy B (2008) An investigation into the high performance of TiN-coated rollers in burnishing process. J Mater Process Tech 207(1–3):350–355

15. Schuha A et al (2007) Deep rolling of titanium rods for application in modular total hip arthroplasty. J Biomed Mater Res B Appl Biomat 81(2):330–335

16. Altenberg I et al (2012) On the effect of deep rolling and laser-peening on the stress-controlled low- and high-cycle fatigue behaviour of Ti-6Al-4 V at elevated temperatures up to 5500C. Int J Fatigue 44:292–302

17. Nalla RK et al (2003) On the influence of mechanical surface treatments—deep rolling and laser shock peening—on the fatigue behaviour of Ti-6Al-4 V at ambient and elevated temperatures. Mater Sci Eng A 355:216–230

18. Bozdana AT et al (2005) Deep cold rolling with ultrasonic vibrations—a new mechanical surface enhancement technique. Int J Mach Tool Manu 45(6):713–718

19. Meyer D et al (2011) Surface hardening by cryogenic deep rolling. Procedia Eng 19:258–263

20. Lin YC et al (2013) Modeling the creep behaviour of 2024-T3 Al alloy. Comput Mater Sci 67:243–248

21. Fattouh M, El-Khabeery MM (1989) Residual stress distribution in burnishing solution treated and aged 7075 aluminium alloy. Int J Mach Tool Manu 29(1):153–160

22. Luo H et al (2006) Study of the burnishing process with cylindrical polycrystalline diamond tool. J Mater Process Tech 180:9–16

23. Luo H et al (2001) Study on the aluminum alloy burnishing processing and the existence of the outstripping phenomenon. J Mater Process Tech 116:88–90

24. Luo H et al (2005) Investigation of the burnishing process with PCD tool on non-ferrous metals. Int J Adv Manuf Technol 25:454–459

25. Yua X, Wangb L (1999) Effect of various parameters on the surface roughness of an aluminium alloy burnished with a spherical surfaced polycrystalline diamond tool. Int J Mach Tool Manu 39:459–469

26. Nestler A, Schubert A (2015) Effect of machining parameters on surface properties in slide diamond burnishing of aluminium matrix composites. Mater Today Proc 2S:S156–S161

27. Hou Y et al (2015) Effect of processing parameters on surface roughness in ultrasonic deep rolling 6061-T6 aluminum alloy with longitudinal-torsional vibration. Appl Mech Mater 722:60–63

28. Ye X et al (2011) Effects of ultrasonic deep rolling on fatigue performance of pre-corroded 7A52 aluminum alloy. Adv Mater Res 189–193:897–900

29. Zhuanga W et al (2014) Deep surface rolling for fatigue life enhancement of laser clad aircraft aluminium alloy. Appl Surf Sci 320:558–562

30. Majzoobi GH et al (2009) The effects of deep rolling and shot peening on fretting fatigue resistance of Aluminum-7075-T6. Mater Sci Eng A 516:235–247

31. Beghini M et al (2014) Experimental parameter sensitivity analysis of residual stresses induced by deep rolling on 7075-T6 aluminium alloy. Surf Coat Tech 254:175–186

32. Al Quran FMF (2015) The effect of roller burnishing on surface hardness and roughness of aluminum alloy. Int J Mech Appl 5(2):37–40

33. Jinlong L, Hongyun L (2013) Effect of surface burnishing on texture and corrosion behavior of 2024 aluminum alloy. Surf Coat Tech 235:513–520

34. Nakamura Y et al (2014) Improvement of fatigue properties in a cast aluminum alloy by roller burnishing and friction stir processing. Adv Mater Res 891–892:662–667

35. Mishra RS et al (1999) High strain rate superplasticity in a friction stir processed 7075 al alloy. Scr Mater 42(2):163–168

36. Mishra RS et al (2003) Friction stir processing: a novel technique for fabrication of surface composite. Mater Sci Eng A 341:307–310

37. Sharma SR, Mishra RS (2008) Fatigue crack growth behavior of friction stir processed aluminum alloy. Scr Mater 59(4):395–398

38. Sharma SR et al (2004) Effect of friction stir processing on fatigue behavior of A356 alloy. Scr Mater 51(3):237–241

39. Ma ZY et al (2010) Superplastic deformation mechanism of an ultrafine-grained aluminum alloy produced by friction stir processing. Acta Mater 58(14):4693–4704

40. Ma ZY et al (2006) Effect of multiple-pass friction stir processing on microstructure and tensile properties of a cast aluminum–silicon alloy. Scr Mater 54(9):1623–1626

41. Vuchkov IN, Vuchkov II (2009) QStatLab Professional, v. 5.5—Statistical Quality Control Software. User's Manual, Sofia

42. Korzynski M (2007) Modelling and experimental validation of the force-surface roughness relation for smoothing burnishing with a spherical tool. Int J Mach Tool Manu 47(12):1956–1964